

## Modern and fossil charcoal: aspects of structure and diagenesis

Ilit Cohen-Ofri <sup>a,\*</sup>, Lev Weiner <sup>b</sup>, Elisabetta Boaretto <sup>c</sup>, Genia Mintz <sup>c</sup>, Steve Weiner <sup>a</sup>

<sup>a</sup> Department of Structural Biology, Weizmann Institute of Science, Rehovot 76100, Israel

<sup>b</sup> Chemical Research Support Unit, Weizmann Institute of Science, Rehovot 76100, Israel

<sup>c</sup> Department of Environmental Science and Energy Research, Radiocarbon Dating Laboratory, Weizmann Institute of Science, Rehovot 76100, Israel

Received 6 June 2005; received in revised form 11 August 2005; accepted 24 August 2005

### Abstract

The structures and compositions of modern and fossil charcoal samples were compared in order to evaluate charcoal degradation processes in archaeological sites. Modern charcoal samples produced in campfires contain two major phases: graphite-like microcrystallites and a non-organized phase. These phases create a mosaic-like structure with differing relative proportions depending on the taxonomic source of the wood used. Fossil charcoal samples (Tel Dor, Israel: 3000 years BP and Kebara Cave, Israel: 40,000 years BP) also contained the graphite-like microcrystallites and the non-organized phases, but were clearly altered compared to modern charcoal. The graphite-like phase of the fossil charcoal has much higher electrical resistivity, and its ESR properties show that it has markedly altered surface electronic states. Infrared spectra show the presence of additional carboxylate groups. Oxidation has therefore altered the structure. This appears to be a “self-humification” process that affects the graphitic component, and probably the non-organized phase as well.

© 2005 Elsevier Ltd. All rights reserved.

*Keywords:* Charcoal; Graphite-like microcrystallites; Degradation; Humic acid; Radiocarbon datings

### 1. Introduction

Organic materials preserved in an archeological site can provide invaluable information on the diet, bedding, housing materials and fuels used by the occupants of the site. Organic materials are also invaluable for radiocarbon dating. Most organic materials are, however, readily degraded by bacteria and fungi, and are therefore not commonly preserved [10]. Only charred organic materials tend to be preserved [18] and are commonly found in many, but significantly not in all archeological sites. Charred materials are thus important components of archaeological sites. We refer here to charcoal preserved in archaeological sites as fossil charcoal.

Charcoal is one form of charred material. It is a product of wood burning either in natural fires, where it can provide information on fire frequencies, that is in turn related to climate, or

on human activities [28]. Its presence in archeological sites in association with hearths and other burned materials may be an indication of the deliberate use of fire by humans [26]. Some of the oldest charcoal thought to be produced by humans dates back to one and a half million years ago [5]. In sites younger than about 400,000 years it can generally be assumed that fire was used and hence the absence of charcoal implies that the manner in which the fire was used did not produce charcoal and/or the charcoal was not preserved. In much younger sites, charcoal may also be the product of various pyrotechnologies such as metal, plaster, ceramic and glass production.

Most of our knowledge of the structure of charred materials (termed char) is due to research on activated carbon for commercial use. These materials are generally produced in ovens at temperatures above 1000 °C, which is significantly higher than the average temperature of a campfire (around 800–900 °C) [20]. In activated carbons the graphite-like layers are referred to as the organized phase. The char also contains a non-organized phase [13] composed of complex aromatic–aliphatic structures [4]. Rosalind Franklin [13] was one of

\* Corresponding author. Tel.: +972 8 9342547; fax: +972 8 9344136.  
E-mail address: [ilit.cohen-ofri@weizmann.ac.il](mailto:ilit.cohen-ofri@weizmann.ac.il) (I. Cohen-Ofri).

the pioneers of this area of research. She used X-ray diffraction to propose a general structure for char (Fig. 1) composed of two phases; a graphite-like phase and a non-organized phase. We use her terminology [13].

In contrast to the study of carbon black produced in ovens at high temperatures, surprisingly little is known about the structure of modern charcoal produced in natural and man made fires [28,7], and almost nothing about the diagenetic processes that affect charcoal once it is buried in sediments. Charcoal is a product of wood burning in an oxygen poor atmosphere. Significant chemical changes take place in the plant material during the charring process [31]. As the temperature increases the major structural components of the wood (hemicellulose, cellulose and lignin) break down while water, CO, CO<sub>2</sub> and other gases are released [31]. The evaporation of these gases results in the condensation of the carbon skeleton and aromatization, which leads to the formation of graphite-like layers [23]. It is known that organic compounds with higher proportions of aromatic compounds typically have higher char yields [6]. This implies that the graphite-like layers will be formed in larger amounts.

Unlike the high temperature charred carbons that are produced in a controlled environment (temperature and pressure), charcoal produced in open fires is very heterogeneous. The charring process is not uniform, and even in a single fire a variety of charcoal types from barely charred to completely charred, are formed. The difference in tree type and hence burning conditions, introduces an additional complication. Charcoal characterization is thus a difficult task.

Little is known about charcoal preservation over time and the causes of its degradation in archeological sites. Charcoal is usually regarded as a relatively inert substance that is not altered by chemical or biochemical processes [22]. A few studies have shown that this may not be the case. Frink [14] showed that the oxidizable carbon (which means the carbons that undergo oxidation with K<sub>2</sub>Cr<sub>2</sub>O<sub>7</sub> – most probably what we refer to as the non-organized phase) present in charcoal samples from an archeological site in New England is variable, and concluded that it had undergone diagenetic changes. Bird et al. [3] demonstrated that the charcoal in Pleistocene strata from an archeological site in Australia (Nauwalabila)

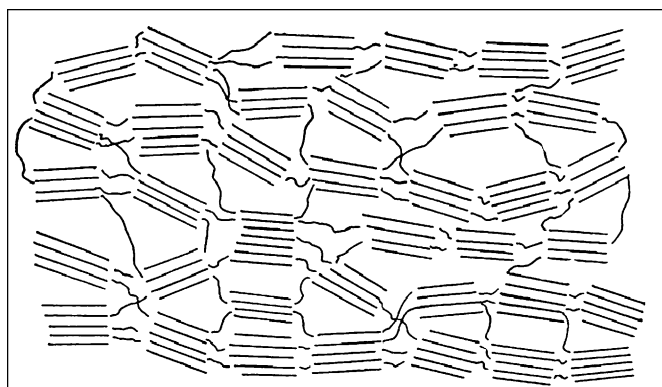


Fig. 1. The proposed structure of carbonized materials showing ordered graphitic structures and a non-organized phase. Adapted from Franklin [13].

was altered. This alteration was viewed in the SEM where the altered charcoals have a degraded internal structure compared to the preserved samples. Their carbon contents also decreased.

One important complication when assessing charcoal degradation is the presence of humic substances. Fossil charcoal is known to contain a certain amount of humic substances. They are extracted during the preparation of charcoal for radiocarbon dating (the Acid–Alkali–Acid (AAA) treatment [24]). These structurally variable aromatic substances are thought to be the degradation products of plants [8] and are believed to penetrate into the charcoal from the surroundings. The general opinion is that humic acids cannot be described in well defined chemical terms. They contain some common molecular blocks [34] that include a nucleus of phenolic groups to which are attached amino acids and aliphatic carbohydrate groups. Widayati and Tan [34] used atomic force microscopy (AFM) to identify hexagonal structured benzene rings with side chains attached to these rings composed of carboxyl and carbonyl groups. Yang and Wang [35] used Raman spectroscopy to show that humic substances from different sources also contain graphite-like layers. Thus soil humic substances may in fact closely resemble charcoal in terms of the presence of graphite-like material and non-organized domains in both materials.

The aim of this study is to improve our understanding of modern charcoal structure, and then compare it to fossil charcoal in order to identify diagenetic processes that alter charcoal with time. The approach used is to first characterize several modern charcoal samples, each produced in a campfire using fresh wood and bark from a specific tree species. These charcoal samples were characterized structurally using a repertoire of techniques that includes transmission electron microscopy, X-ray diffraction, Raman and infrared spectroscopy, electron spin resonance (ESR), resistivity and TGA/DTA. The same methods were then used to characterize fossil charcoal samples from two archeological sites and by comparing the modern and fossil charcoal structures, determine the nature of some of the diagenetic degradation processes.

## 2. Materials and methods

### 2.1. Materials

#### 2.1.1. Modern charcoal sample preparation

A series of modern charcoal samples (Table 1) of known taxonomic origin were produced in open fires on a clean rocky

Table 1  
Charcoal samples prepared from different tree species and the maximum temperature of the fire measured using a thermocouple

No.	Tree species	Max. temp. (°C)
1.	Oak – <i>Quercus caliprinos</i>	950
2.	Carob – <i>Ceratonia siliqua</i>	938
3.	Bay – <i>Laurus nobilis</i>	850
4.	Olive – <i>Olea europaea</i>	937

substrate. They were treated with 1 N HCl in order to remove the remaining ash, washed twice with deionized water and centrifuged at 3000 rpm and finally dried in an oven at 60 °C. The samples were homogenized by gently crushing and grinding in an agate mortar and pestle, and then sieved to <250 µm. These samples were used as the standards for the characterization of modern charcoal. See Schiegl et al. [25] for details.

### 2.1.2. Fossil charcoal sample preparation

The samples are from the Iron Age strata of Tel Dor, Israel (3000 BP) [32] and the Mousterian and early Upper Paleolithic strata of Kebara Cave, Israel (50,000–40,000 BP) [2]. The latter are from the southern part of the cave. These represent two extreme archaeological environments of preservation. Tel Dor sediments almost always contain calcite, which is indicative of an alkaline environment, whereas in Kebara Cave only the sediments in the northern part of the cave contain calcite. The sediments in the center and southern parts contain authigenic phosphate minerals that indicate that the paleo-pH was once around 4–5 [24].

Each sample is a single piece of charcoal. The samples were homogenized by gently crushing and grinding in an agate mortar and pestle, and then sieved to less than 250 µm. The samples were divided into two. One part was left as is and the other was treated with 1 N HCl for half an hour in order to dissolve associated minerals such as calcite. The treated samples were cleaned with deionized water and dried. This was repeated and the weight loss was noted.

## 2.2. Methods

### 2.2.1. Transmission electron microscopy (TEM)

The charcoal samples were sonicated using a powerful instrument (Heat Systems, Farmingdale, NY). The samples were sonicated while floating in a cup horn to avoid heating for 3 min in ethanol. After an additional 2 min to allow for the heavy particles to settle, a drop of the supernatant was placed on a holey carbon coated TEM grid. The particles were examined using a Philips CM120 Super Twin (120 kV) and Philips-FEI Tecnai F30 (300 keV-FEG) microscope.

### 2.2.2. Raman spectroscopy

Measurements were made in air at room temperature using a Renishaw 2000 Raman Imaging Microscope through a 50× lens without a polarizer. The excitation at 632 nm was produced by a 25 mw HeNe laser. Each measurement was made 18 times at random locations on a pellet of the powdered charcoal, and the maximum peak height and peak position were determined and averaged.

### 2.2.3. Fourier transform infrared spectroscopy (FTIR)

FTIR was performed using a Midac Corporation (Costa Mesa, CA, USA) instrument. The spectra were obtained by mixing about 0.1 mg of sample with about 80 mg of KBr. Spectra were collected at 4 cm<sup>-1</sup> resolution.

### 2.2.4. X-ray diffractometry

X-ray powder diffraction patterns were collected using a Rigaku Rotoflex-RU 200 B automatic diffractometer using Cu Kα radiation. The sample was mounted on a germanium crystal to minimize baseline rise.

### 2.2.5. Thermogravimetric and differential thermal analysis (TGA & DTA)

Five milligrams of each charcoal sample was placed in a platinum pan and heated to 1000 °C together with an empty reference pan. The heating was performed in an air atmosphere, with a heating rate of 20 °C/min using a Shimadzu DTG-50 instrument equipped with a microbalance. The baseline spectrum, obtained under the same conditions with two empty platinum pans, was subtracted from the measurement spectrum. The weight loss and the heating temperatures were recorded.

### 2.2.6. Electrical resistivity

The measurements were made using a Teflon cylindrical cell with an outer diameter of 40 × 20 mm and an inner diameter of 4 mm, and electric contacts made of copper. The electrical resistivity was measured using the two-lead technique (in which the voltage drop is measured by the same probe that produces the current excitation), and the measuring instrument was a digital multimeter. The charcoal powder was compressed using a miniature compression device (modified Minimat (Rheometrics, USA)) and the electric resistivity was measured as a function of the force applied to the sample ( $F$ ) and the compression of the cell ( $l$ ). An example for one charcoal sample is shown in Fig. 2. Since the resistance  $R$  ( $\Omega$ ) is  $R = \rho D/A$ , (when  $D$  is the length (m),  $A$  is the cross-section area (m<sup>2</sup>) and  $\rho$  is the electric resistivity ( $\Omega^{-1} \text{m}^{-1}$ )) and  $l$  and  $R$  are measured, we calculate the electric resistivity ( $\rho$ ) from the slope of the curve where the resistance is linear (between 115 and 150 m<sup>-1</sup>) (Fig. 3). This is the zone where the charcoal particles interact with each other and not with air.

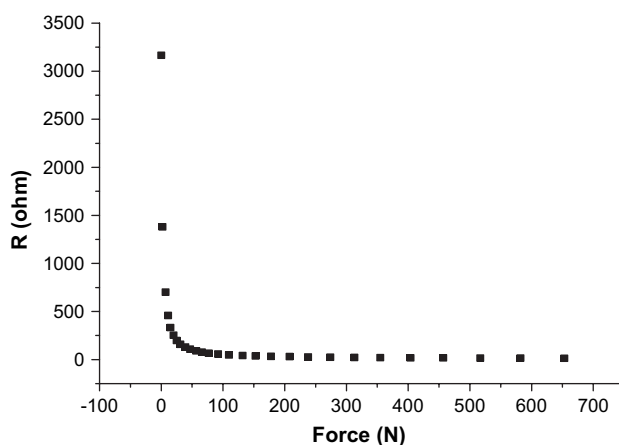


Fig. 2. Electrical resistivity of modern charcoal (*Ceratonia*) in ohms as a function of force in Newtons applied to the powdered sample.

### 2.2.7. Electron spin resonance (ESR)

We used 20 mg of sample for a measurement. For the vacuum experiments the sample was first placed in a vacuum of around  $2 \times 10^{-2}$  torr, sealed and measured. ESR measurements were performed on a Bruker ER 200 D-SRC instrument. The temperature was adjusted by a temperature unit control (Eurotherm, B-VT 2000) with an accuracy of  $\pm 1$  K. A solid sample of  $\text{CuSO}_4 \times 5\text{H}_2\text{O}$  of known weight and number of spins/gr was used as a standard for estimation of concentration of paramagnetic centers by double integration of ESR signals. The accuracy of integration was 20%.

## 3. Results

We used a series of analytical techniques to characterize modern and fossil charcoal structures. The transmission electron microscope provides direct images of the structure at very high resolution. X-ray diffraction and electron spin resonance also provide information on charcoal structure. Raman spectroscopy, infrared spectroscopy, electrical resistivity and differential thermal analysis are more quantitative, but are also more difficult to interpret structurally. Tables 3 and 4 show the results for the modern and fossil charcoal samples using TGA/DTA, resistivity and ESR.

### 3.1. Transmission electron microscopy (TEM)

TEM images (Fig. 4A, B) show the basic structural motif of modern charcoal samples produced in an open fire. The charcoal is clearly composed of microcrystallites revealed by their lattice fringes that have spacings similar to graphite (lattice spacing of  $2.5 \pm 0.3$  Å and also an interlayer spacing of  $3.5 \pm 0.2$  Å). These ordered domains are surrounded by non-organized organic material. The graphite domains and the non-organized domains are also present in the fossil charcoal sample (Fig. 4C, D).

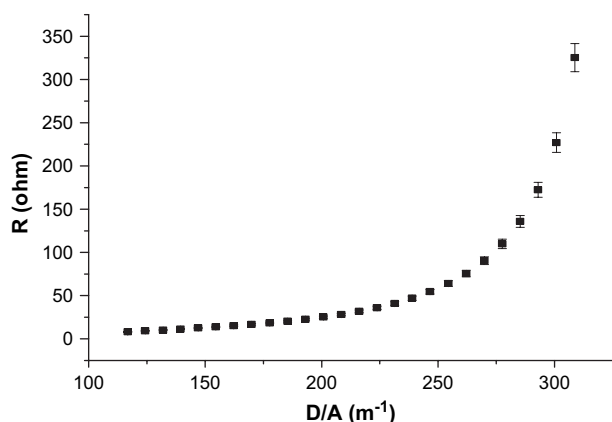


Fig. 3. Electrical resistivity of modern charcoal (*Ceratonia*) in ohms as a function of length in  $\text{m}^{-1}$ . The linear area (between 115 and 150  $\text{m}^{-1}$ ) is used for the determination of the resistivity.

### 3.2. Raman spectroscopy

Fig. 5 shows a characteristic spectrum of charcoal with a peak characteristic of graphite at  $1575 \text{ cm}^{-1}$  (the G peak) and a peak at  $1355 \text{ cm}^{-1}$  which is known as the D peak (D for disorder). The ratio between the two peaks has been used to estimate the domain size of the graphitic areas [33]. Using this formula we determined that the average size of the crystallites is around 4.5 nm (Table 2) for the 4 modern charcoal samples. This is in agreement with the sizes seen on the TEM images. The width and peak positions of the 4 different charcoal samples vary (Table 2) indicating differences in their structures. The fossil charcoal Raman spectra (Fig. 6) have high levels of fluorescence (before and after HCl treatment), as indicated by the intensity values. The G and D peaks are both usually present, but their shapes are somehow influenced by the extent of fluorescence. See also Alon et al. [1].

### 3.3. X-ray diffraction

Fig. 7 is a representative powder diffraction pattern of a modern charcoal sample. It contains only one broad peak centered around the strongest graphite reflection. This confirms that the graphite crystallites are very small. It was not possible to estimate their average size from the diffraction pattern using the Scherer formula because the signal to noise ratio was too small.

### 3.4. Thermogravimetric and differential thermal analysis (TGA/DTA)

Fig. 8 is a representative TGA/DTA plot of a modern charcoal sample. The TGA plot shows that the total weight loss during pyrolysis is above 95%. The DTA plot shows that the major phase change (as reflected by the apex of the peak) occurs around 500 °C. DTA analysis of pure geological graphite (from Eckert Mineral Research) shows that it decomposes around 800–900 °C based on the location of the major peak (not shown). We note that in the modern charcoal samples there is no phase change in this temperature range. We assume that the small size of the charcoal graphite-like crystals reduces the pyrolysis phase change temperature. The 4 modern charcoal samples differ with respect to their DTA maximum temperatures (Table 3). These differences presumably reflect structural differences in the graphite-like crystals. The fossil charcoal samples from Tel Dor undergo a phase change in the same temperature range as the modern samples, and they also vary from one sample to another (Table 4). This is true for the fossil charcoal before and after HCl treatment although the temperatures of the major phase change after HCl treatment are lower. They are similar to or lower than the lower DTA temperatures of a modern charcoal sample (*Olea*). The weight loss during pyrolysis of the fossil charcoal samples is less than that of the modern samples, probably due to a higher proportion of contaminating sediment before HCl treatment.

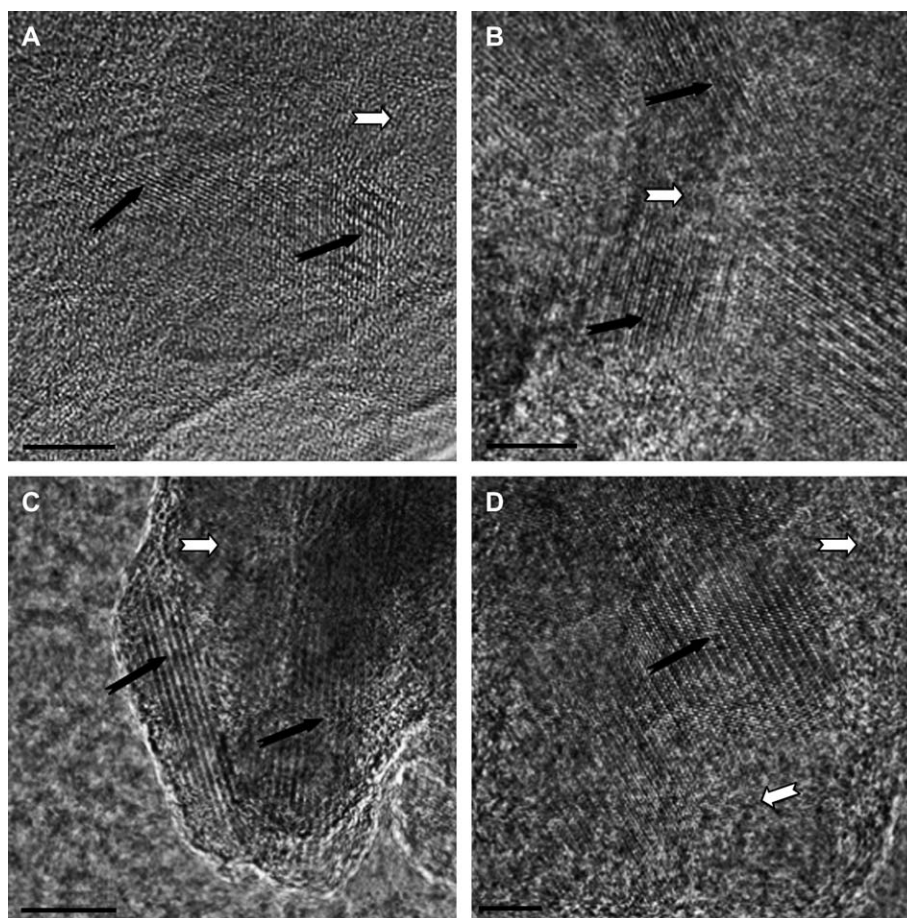


Fig. 4. High resolution TEM images of charcoal showing the lattice fringes of the crystalline graphite domains surrounded by non-organized material. A, B – modern charcoal of *Quercus caliprinos*. C, D – fossil charcoal *Quercus* (scale bar: 5 nm). Black arrows indicate the graphite-like microcrystallite domains and the white arrows are the non-organized phases.

After the treatment the weight loss is the same as in the modern charcoal.

The relative proportions of the non-organized material can be roughly estimated by the weight loss in the temperature range between 200 and 450 °C assuming that the graphite

component burns at the higher temperatures. In modern charcoal this is around 20% of the total weight of the charcoal. In the fossil charcoal samples it is up to 30%. This indicates an increase in the amount of disordered organics in the fossil charcoal, which is consistent with the DTA results.

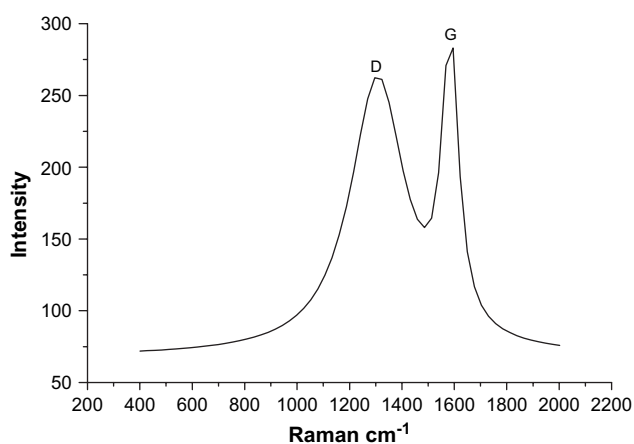


Fig. 5. Raman spectrum of a modern charcoal sample (*Olea*). The 2 distinct peaks ascribed to graphite (G) at 1590  $\text{cm}^{-1}$  and disordered (D) at 1355  $\text{cm}^{-1}$  are shown.

### 3.5. Electrical resistivity

Electrical resistivity can be indicative of the relative amounts of microcrystalline graphite-like components in the charcoal, as graphite is a conductive material. Note that resistivity is the inverse of conductivity. The non-organized organic component is probably less conductive or is a non-conductive phase, whose presence reduces the conductivity. Thus the more conductive the charcoal, the higher the amount of microcrystalline graphite. The range of the electrical resistivity values obtained for the 4 modern charcoal samples is less than  $1\ \rho$  ( $\Omega\text{m}$ ), meaning that they are extremely conductive (Table 3). Fossil charcoal, on the other hand, is an insulator as its resistivity is so high that it hardly conducts (Table 4). Surprisingly even after the removal of the calcite and other carbonates by the HCl treatment, the resistivity did not decrease, but sometimes even increased. This shows that

Table 2

Raman spectroscopy analysis showing the calculated dimension of the graphitic microcrystallites  $L_a$  ( $(I_D/I_G) = 1/(L_a)$ ) and the widths and positions of the D and G peaks

Sample	$L_a$ (nm)	Width – D ( $\text{cm}^{-1}$ )	Width – G ( $\text{cm}^{-1}$ )	Peak D ( $\text{cm}^{-1}$ )	Peak G ( $\text{cm}^{-1}$ )
<i>Olea</i>	$4.9 \pm 0.6$	$269.1 \pm 29.0$	$72.6 \pm 5.1$	$1300.0 \pm 30.9$	$1582.0 \pm 17.3$
<i>Ceratonia</i>	$4.6 \pm 0.4$	$245.4 \pm 15.9$	$71.5 \pm 3.4$	$1301.5 \pm 6.9$	$1583.4 \pm 4.7$
<i>Laurus</i>	$4.6 \pm 0.4$	$239.0 \pm 12.0$	$69.9 \pm 3.9$	$1304.2 \pm 6.6$	$1584.0 \pm 3.8$
<i>Quercus</i>	$4.3 \pm 0.2$	$222.5 \pm 13.8$	$67.0 \pm 2.4$	$1318.8 \pm 5.7$	$1595.0 \pm 3.3$

significant changes have occurred in the fossil charcoal structure compared to modern charcoal with respect to the conducting capability of the graphite component.

### 3.6. Fourier transform infrared spectroscopy (FTIR)

The FTIR spectra of the modern charcoal samples are all very similar (Fig. 9). In general modern charcoal absorbs weakly in the infrared range. There is one broad peak at  $1578 \text{ cm}^{-1}$  that is ascribed to the aromatic C=C ring stretching [23]. Comparing the spectra we obtained to those of Nishimiya et al. [23], we conclude that our samples formed in the temperature range between 600 and  $800 \text{ }^\circ\text{C}$ . This is consistent with the actual temperatures measured in open fires [20]. What remains of the non-organized fraction is mostly aromatic groups, which were probably dehydrated and deoxidized [23]. The fossil charcoal spectra (Fig. 10) absorb much more in the infrared range, and have well defined peaks that are ascribed to charged carboxylate groups ( $\text{COO}^-$  at  $1597 \text{ cm}^{-1}$  and  $1400 \text{ cm}^{-1}$ ). After treatment with HCl (Fig. 11) the  $1597 \text{ cm}^{-1}$  peak divides into two peaks at  $1618 \text{ cm}^{-1}$  and a COOH peak at  $1710 \text{ cm}^{-1}$ .

### 3.7. Electron spin resonance (ESR)

ESR detects the presence of unpaired electrons (paramagnetic centers), that in charcoal are associated mainly with organic molecules rather than transition metal ions. Unpaired electrons associated with organic molecules are called free

radicals [21,27]. ESR can thus provide detailed information on the atomic structure of such materials, which includes graphite [30]. The presence of unpaired electrons in natural charcoals is well-documented [17,7]. It is thought that free radicals in charcoals are produced as a result of thermal damage of normal carbon–hydrogen bonds during the formation of condensed carbon rings [17]. During this process the unpaired electrons are stabilized by the cyclic carbon  $\pi$ -system.

Fig. 12a shows the signals obtained for the 4 modern charcoal samples after the air was removed by placing the samples in a vacuum. This treatment removes the oxygen and reduces its magnetic (dipole–dipole) influence on the paramagnetic centers of the charcoal. The 4 modern charcoal samples all have basically the same shaped signal, but the extent of broadening varies. The *Ceratonia* sample produced the narrowest signal and the *Quercus* sample the broadest. Emmerich et al. [11] have shown that this broadening can be attributed to the presence of narrow and a broad components in the charred samples they examined. The signal that contributes mainly to the narrow component is affected by changing the measurement temperature, whereas the broad signal is not affected. This means that the narrow component contribution behaves in a Curie–Weiss manner (Figs. 12b and 13). This behavior is characteristic of free radicals i.e. unpaired electrons. The broad line component is characteristic of free charge carriers (near Pauli paramagnetism), which are believed to be localized on the graphitic microcrystallites [11]. We confirmed the same behavior for the *Quercus* and the *Ceratonia* modern charcoals.

A well defined parameter of an ESR spectrum is the so-called  $g$ -value, which is dependent on the atomic and crystallographic system in which the electron is located. It is

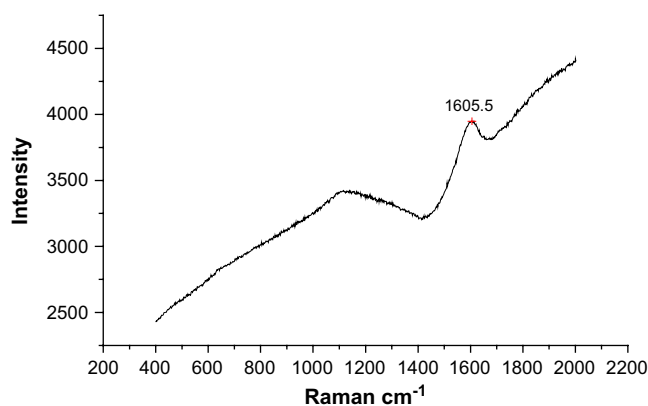


Fig. 6. Raman spectrum of a fossil charcoal sample (Kebara Cave). The G peak at  $1605.5 \text{ cm}^{-1}$  is present, but the D peak at  $1355 \text{ cm}^{-1}$  is not. Note the very high intensity due to fluorescence as compared to the modern charcoal sample (Fig. 5).

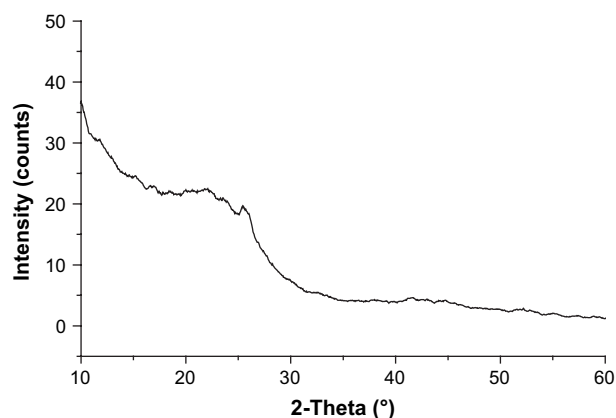


Fig. 7. Powder X-ray diffraction pattern of modern charcoal (*Ceratonia*). The broad peak indicates the presence of very small crystals.

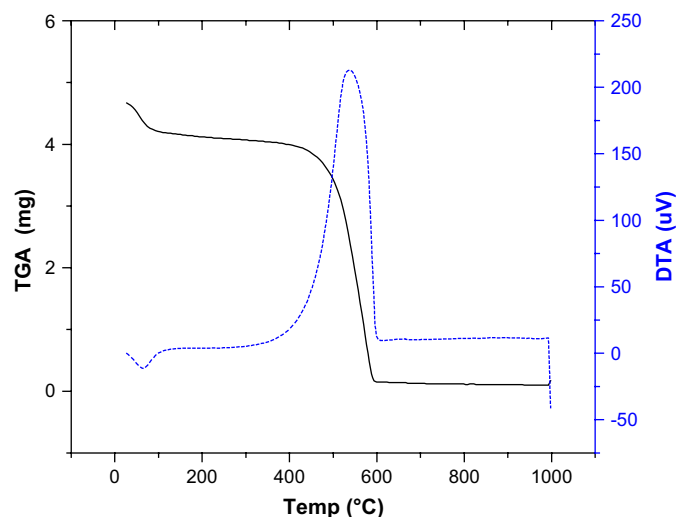


Fig. 8. TGA/DTA plots of modern charcoal (*Ceratonia*) heated to 1000 °C (solid line: TGA, dashed line: DTA).

therefore characteristic of a particular atomic site. Schurr et al. [27] showed that in pyrolysed plants the  $g$ -value is related to the remaining oxygen, and as the pyrolysis temperature increases, the  $g$ -value decreases and approaches  $g_0$ . The  $g_0$  value is that of a free electron and has a value of 2.0023. Table 3 shows the  $g$ -values for the 4 modern charcoal samples. These values have small but significant differences. As the values are close to the value of a free electron, we conclude that the signal in modern charcoal is mainly derived from the free electrons associated with aromatic  $\pi$  radicals in both phases [11]. We also conclude that the *Quercus* sample was formed at the highest temperature as it has the largest amount of free charge carriers. The latter, according to Singer and Wagoner [30], are located only in the graphite-like microcrystallites. The concentration of the paramagnetic centers was found to be  $10^{18}$  spin/mg (Table 3). We also examined the dependence of the ESR signal intensity on microwave power (saturation curves). The modern sample did not reach saturation (Fig. 14). This can be explained by a high local concentration of paramagnetic centers, that makes spin-lattice relaxation time ( $T_1$ ) shorter. In general, the ESR characteristics of modern charcoal are dominated by the behavior of free electrons associated with both the graphite and the non-organized phases, and free charge carriers associated only with the graphite-like microcrystallites.

The fossil charcoal ESR signal after treatment in vacuum and HCl is broad,  $\Delta H = 8G$  (Fig. 15). The concentration of

the paramagnetic centers is more than 2 orders of magnitude less than the concentration in modern charcoal ( $10^{16}$  spins/gr) before treatment with HCl and 1 order of magnitude less ( $10^{17}$  spins/gr) after treatment with HCl. The fossil charcoal  $g$ -value ( $\sim 2.0034$ ) is higher than that of modern charcoal ( $\sim 2.0023$ ) (Table 4). We note that this difference in  $g$ -values is significant and is indicative of different chemical environments. This implies that some of the radicals are not located in an aromatic environment since their  $g$ -values no longer reflect the environment of free radicals. The latter is stabilized in an aromatic environment. The fossil charcoal does saturate (Fig. 16) thus revealing a completely different behavior as compared to modern charcoal. This means that these samples have a relatively long relaxation time ( $T_1$ ). This behavior is characteristic of “diluted” spin systems which couple weakly with the surroundings. Clearly the atomic structure of the graphitic microcrystallites has been radically altered in the fossil charcoal due to some diagenetic processes.

#### 4. Discussion

Both the modern and the fossil charcoal samples comprise two different phases; a crystalline phase composed of graphite-like microcrystals, and a non-organized phase. Despite this, the analyses of modern and fossil charcoals reveal differences, some of which are most striking. Here we first discuss modern charcoal structure and then fossil charcoal structure, and by comparing the two, we identify some of the prominent diagenetic processes that affect fossil charcoal.

##### 4.1. The influence of HCl treatment

The treatment with HCl removes the carbonates (mostly ash calcite) and makes possible the examination of the charcoal alone. This treatment in modern charcoal indeed removed only calcite (as shown by FTIR). In fossil charcoal, however, the HCl treatment may have an additional, as yet not understood effect that results in the release into solution of some of the degradation products.

##### 4.2. Modern charcoal structure

The TEM images clearly show that Franklin’s model [13] for charcoal formed at high temperatures (Fig. 1) is basically applicable to charcoals formed in natural fires. The major difference is that the proportion of the non-organized phase in the

Table 3  
Analyses of the 4 modern charcoal samples using electronic resistivity –  $\rho$  ( $\Omega\text{m}$ ) ( $n = 3$ ), DTA peak location ( $^{\circ}\text{C}$ ) and TGA weight loss in % ( $n = 5$ ), the  $g$  values and spin concentration obtained from ESR measurements

Sample	$\rho$ ( $\Omega\text{m}$ )	DTA ( $^{\circ}\text{C}$ )	TGA (weight loss%)	$g$	Concentration (spins/gr) $\times 10^{18}$
<i>Olea</i>	$0.998 \pm 0.159$	$491.4 \pm 2.1$	$95.6 \pm 2.2$	2.0018	5.8
<i>Ceratonia</i>	$0.146 \pm 0.021$	$536.2 \pm 2.5$	$97.3 \pm 1.1$	2.0017	5.2
<i>Laurus</i>	$0.032 \pm 0.003$	$559.0 \pm 4.1$	$97.5 \pm 1.0$	2.00215	9.3
<i>Quercus</i>	$0.015 \pm 0.002$	$549.6 \pm 4.6$	$97.9 \pm 0.4$	2.0020	6.7

The concentrations of spins using ESR are calculated in comparison to  $\text{CuSO}_4 \times 5\text{H}_2\text{O}$  standard.

Table 4

Analyses of fossil charcoal samples from Tel Dor before and after HCl treatment. ((a) electrical resistivity –  $\rho$  ( $\Omega\text{m}$ ), DTA peak location – ( $^{\circ}\text{C}$ ) and TGA weight loss – %; (b) showing ESR  $g$  value and spin concentration (spins/gr) calculated in comparison to  $\text{CuSO}_4 \times 5\text{H}_2\text{O}$  standard)

(a)							
Sample	Location	$\rho$ ( $\Omega\text{m}$ )	$\rho$ ( $\Omega\text{m}$ ) HCl	DTA ( $^{\circ}\text{C}$ )	DTA ( $^{\circ}\text{C}$ ) HCl	TGA (%)	TGA (%) HCl
CHI-4	Area D2	252,254	37,959	549	504.5	83	96
CHI-5	Area D2	49,982	34,073	540	493.7	77.5	95
CHI-9	Area D2	17,434	47,372	521	453.5	88.7	100
CHI-12	Area G	395,447	64,280	493	454	71	100
CHI-23	Area G	461,473	47,372	501	446	74	93
WD2F-8	Area G	235,499	299,621	505	463	92	100
(b)							
Sample	$g$	$g$ HCl	Conc. (spins/gr) $\times 10^{18}$	Conc. (spins/gr) $\times 10^{18}$ HCl			
CHI-4	2.0037	2.0034	0.078	0.41			
CHI-5	2.0035	2.0033	0.17	0.21			
CHI-9	2.0036	2.0031		0.06			
CHI-12	2.0037	2.0034	0.027	0.11			
CHI-23	2.0038	2.00305	0.061	0.1			
WD2F-8	2.0040	2.0032		0.19			

latter is much higher due to the lower temperatures at which the natural charcoals form. The graphite microcrystallites are very small in modern charcoal. Direct observations by TEM, as well as indirect observations by Raman spectroscopy indicate that the average crystallite size of the sheets is around 4–5 nm. We know very little about the chemical structure of the disordered organic component. It has been suggested that aromatic groups are common [23]. Clearly much still remains to be understood about the chemical nature of this component and how it is bound to the graphite-like crystallites.

In general the 4 samples of modern charcoal analysed here are similar. We did, however, detect small but significant differences that probably reflect mainly varying proportions of the two different phases. This is especially apparent in the DTA measurements. We assume that the lower the temperature of the major DTA peak, the larger is the proportion of the disordered organic component. This assumption is supported by the relation between electrical resistivity and the major DTA phase change temperature (Fig. 17). The larger the relative

amount of non-organized organics, the higher is the electric resistivity, since this phase probably interrupts the contacts between the graphite-like microcrystallites. Both the electrical resistivity and the ESR measurements provide information on the organization and on the atomic structure of the graphite-like component. They support the notion that the graphite-like component closely resembles geological graphite, except for the small size of the crystallites. We did note variations in the graphite-like crystallite properties (mainly peak widths) using Raman spectroscopy. As the narrower the peak, the more it resembles geological graphite, we conclude that the most ordered graphite component is present in *Quercus*, then in *Laurus*, followed by *Ceratonia* and the least ordered graphite component is present in the *Olea* sample. These differences are also detected by the ESR measurements. The *Quercus* charcoal sample, which is also the most conductive sample, contains the most free electron charge carriers. These are formed at higher temperatures and contribute to the reduction in electric resistivity. This again implies that the *Quercus*

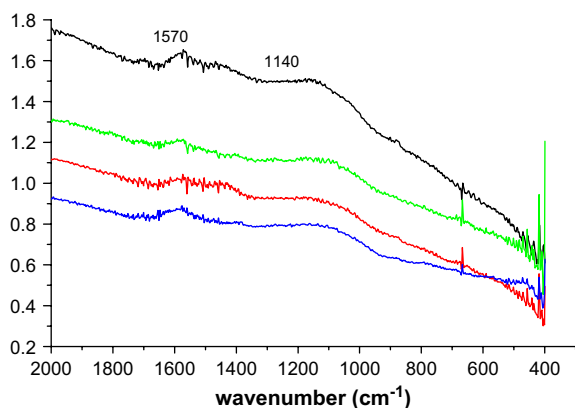


Fig. 9. FTIR spectra of the 4 modern charcoal samples. The peak at  $1570\text{ cm}^{-1}$  is the C=C aromatic stretching.

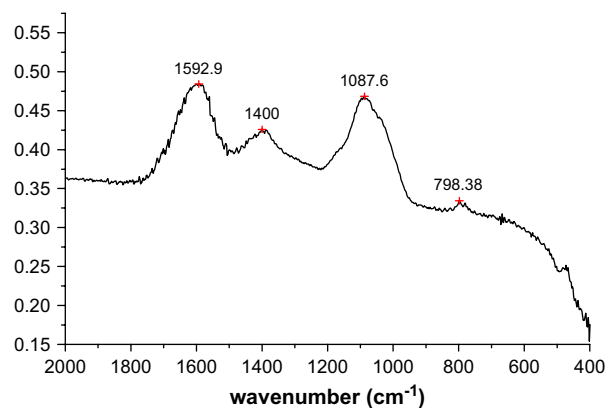


Fig. 10. FTIR spectrum of fossil charcoal (collected from Kebara Cave). The sample contains carboxylate groups ( $1583$  and  $1400\text{ cm}^{-1}$ ) and a mineral phase (quartz) ( $1087$ ,  $798$  and  $778\text{ cm}^{-1}$ ).

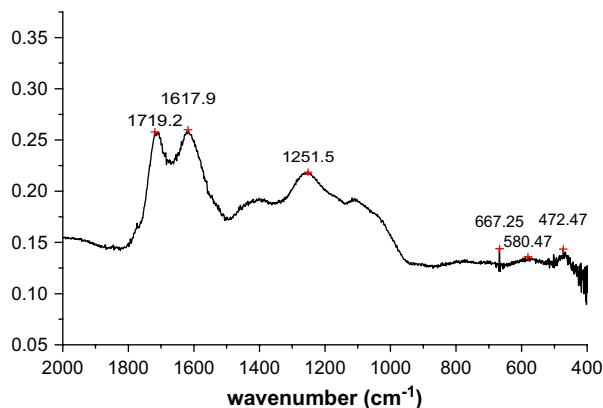


Fig. 11. FTIR spectrum of fossil charcoal (Kebara Cave) after treatment with 1 N HCl. The sample contains peaks due to carboxylic acids ( $1719\text{ cm}^{-1}$ ) and carboxylate groups ( $1617$ ,  $1400$  and  $1251\text{ cm}^{-1}$ ).

sample contains larger amounts and/or more ordered graphite microcrystallites. We do not know what properties of burning oak are responsible for this difference.

We conclude that modern charcoal is, as described previously [13], composed of two phases: an organized phase,

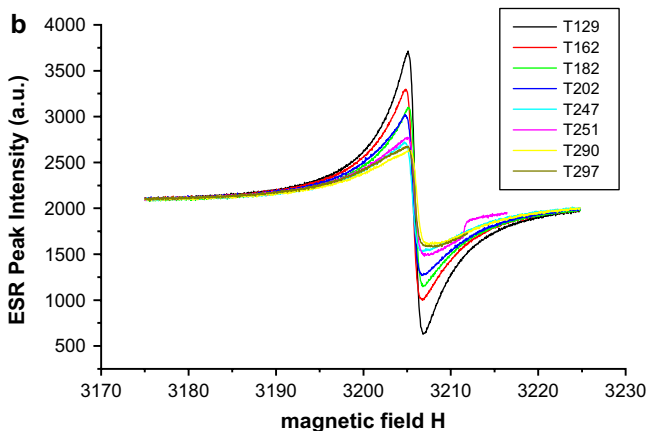
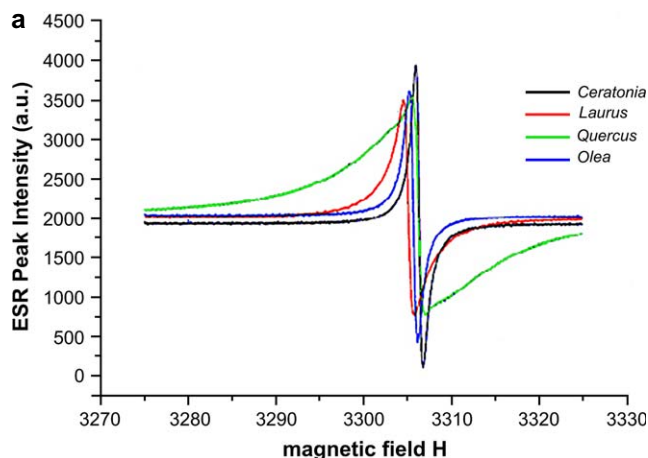


Fig. 12. (a) ESR signals of the modern charcoal samples under vacuum. Note that the *Quercus* sample contains an additional peak. (b) ESR signal of *Quercus* sample under vacuum at different temperatures (the temperatures are in degrees Kelvin). This measurement establishes the temperature dependence of the ESR signal.

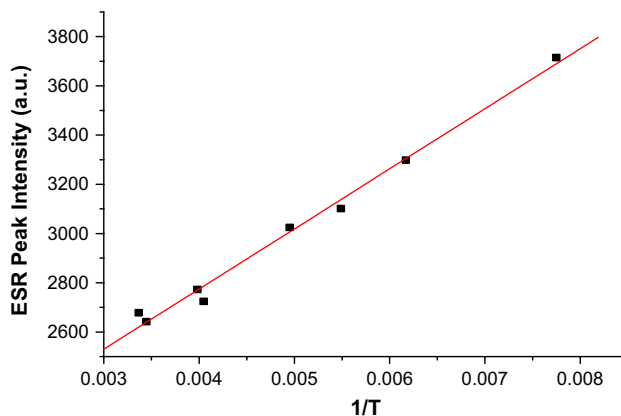


Fig. 13. The linear dependence between the temperature and the peak height in the *Quercus* charcoal sample indicates a Curie–Weiss behavior of the free radicals.

which is composed of graphite-like microcrystallites, and a non-organized phase. These two phases are connected and the relative amounts of each change the charcoal properties. We use this model of charcoal to better understand the degradation processes in fossil charcoal.

#### 4.3. Fossil charcoal structure

As graphite is one of the most stable materials in nature [9], our initial hypothesis was that fossil charcoal samples will contain a larger proportion of graphite-like microcrystallites compared to modern charcoal, and that the non-organized phase will be reduced as it is most susceptible to diagenetic degradation. In fact almost all the measurements we made on fossil charcoal point to the opposite scenario, namely the fraction that degrades most is the graphite-like phase.

The fossil charcoal samples clearly do have a crystalline graphite-like phase. This is directly observed in the TEM and indirectly inferred from the Raman spectra. Its electrical properties are, however, severely altered. The huge increase

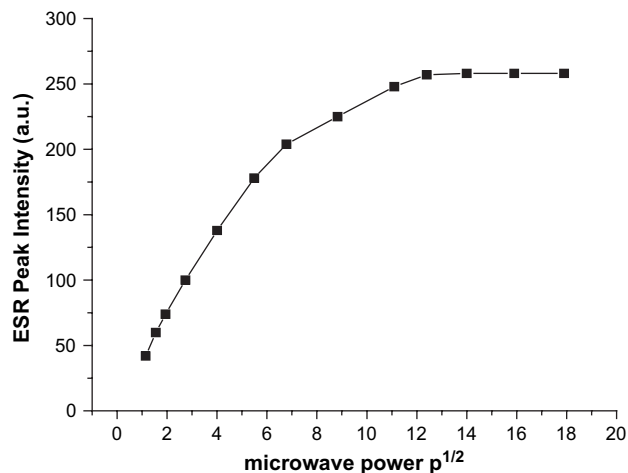


Fig. 14. The saturation curve of modern charcoal (*Ceratonia*). The sample does not reach saturation.

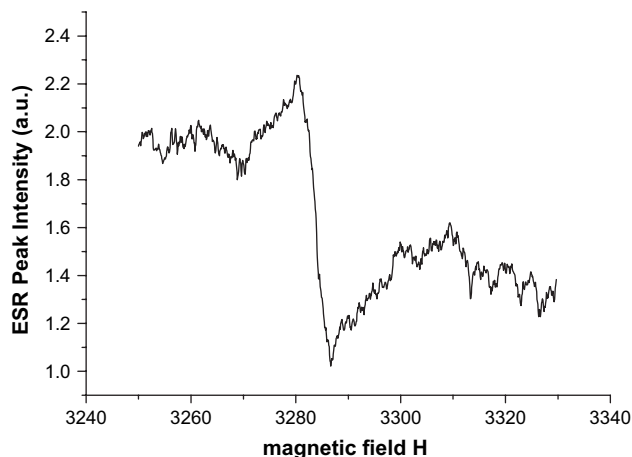


Fig. 15. ESR signals of the fossil sample (Tel Dor, CHI-9) after HCl treatment under vacuum. This spectrum is broader than the modern charcoal spectrum.

in electrical resistivity compared to the modern charcoal shows that this phase is almost incapable of conducting electrons. The ESR analyses provide information on the atomic environment of the graphite-like crystallite, and these also show that it has been drastically altered. The concentration of free electrons decreased by 1 order of magnitude, and the local environment in which they exist is quite different (as inferred from the higher ESR  $g$ -values and the saturation behavior of the fossil samples).

The infrared spectra provide the most direct evidence pertaining to the actual change. The fossil samples have distinct carboxylate absorptions that are not present in the modern samples. This implies that the charcoal has undergone oxidation. Although we do not have direct proof that this oxidation affected the graphite phase, the observed changes are consistent with the graphite crystallite surfaces undergoing oxidation and thus affecting free electron movement and hence resistivity.

The relative proportion of the non-organized phase of the fossil samples appears to increase, based on the trends observed mainly from the TGA and DTA analyses. The TGA analyses point to an increase of about 10 weight% of this

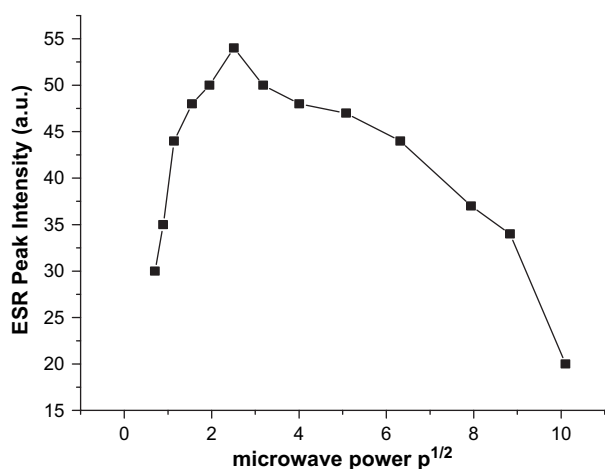


Fig. 16. The saturation curve of fossil charcoal (Tel Dor, CHI-9). This is an example of a sample that saturates.

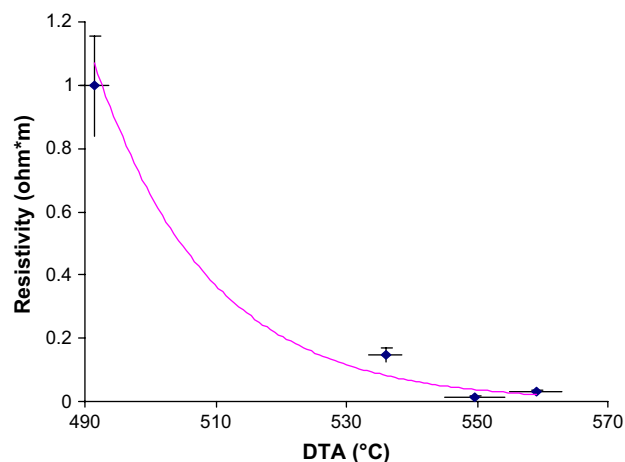


Fig. 17. Electrical resistivity measurement vs. DTA maximum phase change temperature of the 4 modern charcoal samples. This shows that the resistivity of the charcoal tends to decrease exponentially.

phase in the samples measured. This in turn raises the question of whether or not this is due to the introduction of humic acids from the surroundings, or due to the breakdown of the graphitic component of the charcoal itself, or both. One indication that breakdown of the graphitic phase most likely occurs is that during the AAA treatment of some fossil charcoals (not those analysed in this study), it has been observed that the alkali extraction steps can remove up to 80 or 90% by weight of the sample. It is unlikely that this can all be attributed to extraneous humic acid contamination. Furthermore, according to Alon et al. [1] the high fluorescence levels detected in the Raman spectra of fossil charcoals are not removed even after several alkali treatments. Since all of the humic substances from external sources should be removable after such treatment, the high fluorescence level is most likely derived from an integral part of the original material. We also observed that Raman spectra of “humic acid” extracted from archaeological charcoal by alkali contain, besides a high level of fluorescence, the two characteristic peaks of graphite, similar to the fossil charcoal samples (Fig. 6). Thus the alkali treatment may also be removing degraded charcoal phases that have disaggregated into fine particles.

All these observations lead us to conclude that charcoal, and in particular the graphitic component, degrades via oxidation into material resembling humic acid. This model is schematically illustrated in Fig. 18. It may be that “humic acid” derived from charcoal differs from soil humic acid by having a crystalline graphitic phase. Haumaier and Zech [15] suggested that as soil humic acid is highly aromatic, it may be derived from charred plant residues. Kumada [19] and Shindo et al. [29] arrived at a similar conclusion after comparing humic acid compositions from charred residues to humic substances from volcanic ash soils. As charcoal is known to be an excellent absorber of ions and other organic molecules, it most likely also contains soil derived humic and fulvic molecules. Our results, however, point to the possibility, that particularly in more degraded fossil charcoal samples, the major source material for increasing the proportion of the non-organized

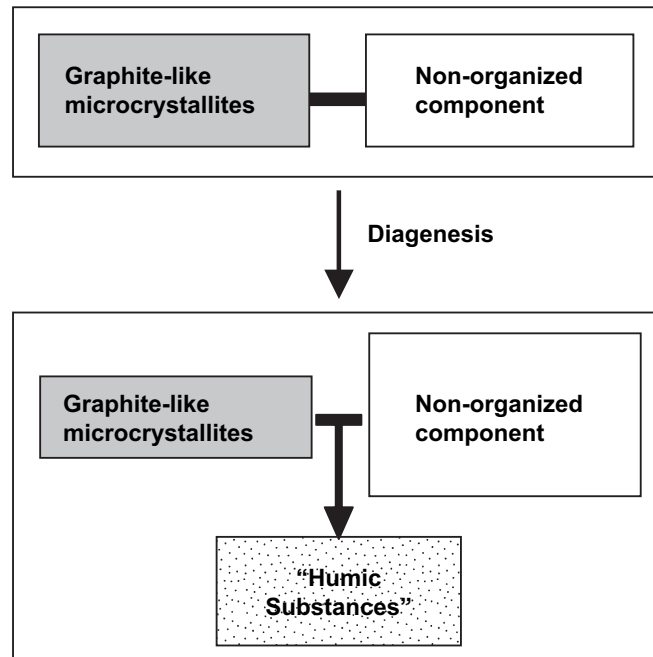


Fig. 18. Schematic representation of the chemical diagenetic model of charcoal. The modern charcoal comprises 2 phases: graphite microcrystallites and a non-organized phase. Diagenesis (mainly oxidation) causes the relative amount of graphite microcrystallites to decrease producing “humic substances” that resemble those in soil.

phase, may be the result of “self-humification” of mainly the graphitic component of the charcoal.

#### 4.4. Broader implications

We have analysed charcoal samples from 3 other sites in Israel (Tel Rehov – 2800–2900 BP, Motza – 9000–9300 BP and Ohalo II– 23,000 BP uncalibrated), and one from Georgia (Ortvale Klde – 21,000–40,000 BP uncalibrated). We found that basically the properties we report here are similar to those we measured for charcoal samples from these sites. We therefore believe that Tel Dor and Kebara Cave specimens are representative of many fossil charcoal specimens.

It is possible that this “self-humification” process is accelerated in a basic environment. In Kebara Cave for example, charcoal is rarely found in sediments with calcite and carbonated apatite (implying a neutral to basic environment), but is more common in sediments that were in an acidic environment [25]. Heinrich [16] found that electrolysis of carbon black under basic conditions produced humic acid, but not under acidic or neutral pH.

In many archaeological sites, and especially in prehistoric caves, black organic-rich layers are present. The diagenetic trends reported here raise the question as to whether at least some of these originate from degraded charcoal. It is interesting to note that in Kebara Cave, one such organic-rich layer contains diatoms and is therefore most likely derived from organic-rich sediment formed in a pool, whereas many of the other organic-rich black layers are intimately associated with hearth structures [2]. These may be derived from charcoal; a subject we are currently investigating.

#### 4.5. Implications for radiocarbon dating

If this model is correct, then much of the material extracted by alkaline treatment of poorly preserved wood charcoal samples, may actually be the original charcoal itself, but in a more degraded form. If this is not contaminated with other carbon sources, it should provide a reliable date. The problem, however, is that such charcoal derived “humic substances” may not be distinguishable from soil derived humic substances. On the other hand, selecting well preserved wood charcoal specimens after HCl treatment based on low resistivity, high DTA transition temperatures or on narrow ESR profiles, and then treating only these with alkali, will improve the chances that the contaminating humic substances will be effectively removed by the alkali and the date obtained will be reliable. In practice, a good criterion for well preserved charcoal may be a sample that loses minimal weight after the alkali extraction steps have removed all the colored substances.

## 5. Conclusions

A comparison of modern and fossil charcoal produced in campfires reveals the following:

1. Both modern and fossil charcoal have basically the same structure: graphite-like microcrystallites and a non-organized phase.
2. The fossil charcoal contains abundant carboxylate groups, which are absent in modern charcoal, implying that diagenesis involves oxidation.

3. The graphite-like phase of the fossil charcoal has higher electrical resistivity, and its ESR properties show that it has a markedly altered surface electronic state. This we attribute to oxidation.
4. The data indicate that the proportion of the graphite phase is reduced during diagenesis relative to the non-organized phase. This may involve a “self-humification” process, whereby the graphite component and possibly the non-organized phase, degrades into humic substances.

## Acknowledgements

We thank Talmon Arad for his expert help with the TEM. We also thank Ofer Bar-Yosef for his help with the Kebara Cave samples, Dan Namdar for the samples from Ohalo II, Amihai Mazar for the Tel Rehov samples, Hamudy Khalaily for the Motza samples and Ilan Sharon and Ayelet Gilboa for the Tel Dor samples. We thank Mr. George Schwartzmann, Sarasota, Florida, for his generous support. We also thank the Kimmel Center for Archaeological Science for their financial support. S.W. is the incumbent of the Dr. Trude Burchardt professorial chair of Structural Biology.

## References

- [1] D. Alon, G. Mintz, I. Cohen, S. Weiner, E. Boaretto, The use of Raman spectroscopy to monitor the removal of humic substances from charcoal: quality control for  $^{14}\text{C}$  dating of charcoal, *Radiocarbon* 44 (2002) 1–11.
- [2] O. Bar-Yosef, B. Vandermeersch, B. Arensburg, A. Belfer-Cohen, P. Goldberg, H. Laville, L. Meignen, Y. Rak, D. Speth, E. Tchernov, A.M. Tillier, S. Weiner, The excavations in Kebara Cave, Mt. Carmel, *Current Anthropology* 33 (1992) 497–550.
- [3] M.I. Bird, C.S.M. Turney, K. Fifield, R. Jones, L.K. Ayliffe, A. Palmer, R. Cresswell, S. Robertson, Radiocarbon analysis of the early archaeological site of Nauwalabila I, Arnhem Land, Australia: implications for sample suitability and stratigraphic integrity, *Quaternary Science Reviews* 21 (2002) 1061–1075.
- [4] S. Blazewicz, A. Swiatkowski, B.J. Trznadel, The influence of heat treatment on activated carbon structure and porosity, *Carbon* 37 (1999) 693–700.
- [5] C.K. Brain, A. Sillen, Evidence from the Swartkrans cave for the earliest use of fire, *Nature* (1988) 464–466.
- [6] C.E. Byrne, D.C. Nagle, Carbonization of wood for advanced materials applications, *Carbon* 35 (1997) 259–266.
- [7] M.J. Cope, Physical and chemical properties of coalified and charcoaled phytoclasts from some British Mesozoic sediments: an organic geochemical approach to palaeobotany, in: A.G. Douglas, J.R. Maxwell (Eds.), *Advances in Organic Geochemistry*, Pergamon Press, Oxford, 1979, pp. 663–677.
- [8] S. Cornelius, What is humic acid? A perspective of the past forty years, in: E.A. Ghabbour, G. Davies (Eds.), *Understanding Humic Substances*, Royal Society of Chemistry, Cambridge, 1999, pp. 1–8.
- [9] M.S. Dresselhaus, The wonderful world of carbon, in: R.P.H. Chang, S. Yoshimura (Eds.), *Supercarbon: Synthesis, Properties and Applications*, Springer, Berlin, 1998, pp. 9–29.
- [10] G. Eglinton, G.A. Logan, Molecular preservation, *Philosophical Transactions of the Royal Society of London B* 333 (1991) 315–327 (discussion 327–328).
- [11] F.G. Emmerich, C. Rettori, C.A. Luengo, ESR in heat-treated carbons from the endocarp of Babassu coconut, *Carbon* 29 (1991) 305–311.
- [12] R.E. Franklin, Crystallite growth in graphitizing and non-graphitizing carbons, *Proceedings of the Royal Society A* 209 (1951) 196–218.
- [13] D.S. Frink, The chemical variability of carbonized organic matter through time, *Archaeology of Eastern North America* 20 (1992) 67–79.
- [14] L. Haumaier, W. Zech, Black carbon – possible source of highly aromatic components of soil humic acids, *Organic Geochemistry* 23 (1995) 191–196.
- [15] T. Heinrich, The oxidation of carbon in electrolytes at normal temperature, *Transactions of the Faraday Society* 34 (1938) 1033–1039.
- [16] D.J. Ingram, *Biological and Biochemical Application of Electron Spin Resonance*, Adam Hilger LTD, London, 1969.
- [17] E.V. Komarek, Ancients fires, in: *Proceedings of Annual Tall Timbers Fire Ecology Conference*, 1973, pp. 219–240.
- [18] K. Kumada, Carbonaceous materials as a possible source of soil humus, *Soil Science and Plant Nutrition* 29 (1983) 383–386.
- [19] A.S. Livingston, Bonfire II: the return of pottery firing temperatures, *Journal of Archaeological Science* 28 (2001) 991–1003.
- [20] S. Mrozowski, ESR studies of carbonization and coalification processes part II. Biological materials, *Carbon* 26 (1988) 531–541.
- [21] G.J. Nichols, J.A. Cripps, M.E. Collinson, A.C. Scott, Experiments in waterlogging and sedimentology of charcoal: results and implications, *Paleogeography, Paleoclimatology, Paleocology* 164 (2000) 43–56.
- [22] K. Nishimiya, H. Toshimitsu, Y. Imamura, Analysis of chemical structure of wood charcoal by X-ray photoelectron spectroscopy, *Journal of Wood Science* 44 (1998) 56–61.
- [23] E.A. Olson, W.S. Broecker, Sample contamination and reliability of radiocarbon dates, *Transactions of the New York Academy Sciences, Series II* 20 (1958) 593–604.
- [24] S. Schiegl, P. Goldberg, O. Bar-Yosef, S. Weiner, Ash deposits in Hayonim and Kebara caves, Israel: macroscopic, microscopic and mineralogical observations, and their archaeological implications, *Journal of Archaeological Science* 23 (1996) 763–781.
- [25] M.B. Schiffer, *Formation Processes of the Archaeological Record*, University of New Mexico Press, Albuquerque, 1987.
- [26] M.R. Schurr, R. Hayes, L.L. Bush, The thermal history of maize kernels determined by electron spin resonance, *Archaeometry* 43 (2001) 407–419.
- [27] A.C. Scott, The pre-Quaternary history of fire, *Paleogeography, Paleoclimatology, Paleocology* 164 (2000) 281–329.
- [28] H. Shindo, T. Higashi, Y. Matsui, Composition of humic acid from charred residues of Susuki (*Eulalia*, *Miscanthus sinensis* A.) and from the A horizons of volcanic ash soils, *Soil Science and Plant Nutrition* 32 (1986) 579–586.
- [29] L.S. Singer, G. Wagoner, Electron spin resonance in polycrystalline graphite, *The Journal of Chemical Physics* 37 (1962) 1812–1817.
- [30] E.J. Soltes, T.J. Elder, *Pyrolysis-Organic Chemicals from Biomass*, CRC Press, 1981.
- [31] E. Stern, *Dor – Ruler of the Seas*, Israel Exploration Society, Jerusalem, 2000.
- [32] F. Tuinstra, J.L. Koenig, Raman spectrum of graphite, *The Journal of Chemical Physics* 53 (3) (1970) 1126–1130.
- [33] S. Widayati, K.H. Tan, Atomic force microscopy of humic acid, *Communications in Soil Science and Plant Analysis* 28 (1997) 189–196.
- [34] Y. Yang, T. Wang, Fourier transform Raman spectroscopy characterization of humic substances, *Vibrational Spectroscopy* 14 (1997) 105–112.